INTERNATIONAL JOURNAL OF
NUMERICAL ANALYSIS AND MODELING
Volume 4, Number 3-4, Pages 342–352

A LEAST-SQUARES METHOD FOR CONSISTENT MESH TYING

PAVEL BOCHEV AND DAVID DAY

Abstract. In the finite element method, a standard approach to mesh tying is to apply Lagrange multipliers. If the interface is curved, however, discretization generally leads to adjoining surfaces that do not coincide spatially. Straightforward Lagrange multiplier methods lead to discrete formulations failing a first-order patch test [12]. A least-squares method is presented here for mesh tying in the presence of gaps and overlaps. The least-squares formulation for transmission problems [5] is extended to settings where subdomain boundaries are not spatially coincident. The new method is consistent in the sense that it recovers exactly global polynomial solutions that are in the finite element space. As a result, the least-squares mesh tying method passes a patch test of the order of the finite element space by construction. This attractive computational property is illustrated by numerical experiments.

Key Words. finite elements, mesh tying, least-squares, first-order elliptic systems

1. Introduction

Mesh tying, or domain bridging, is the opposite of substructuring. A substructuring method solves a boundary value problem using subdomains formed by clustering finite elements from a given discretization of a domain Ω. A mesh tying method solves the same problem by using a discretization of Ω, composed of subdomains that were meshed completely independently. The weak problem is obtained by joining subdomain problems through a suitable variational principle. The simplest nontrivial case of mesh tying is as follows. Assume that Ω is an open bounded domain with Lipschitz continuous boundary Γ, composed of two subdomains; $\overline{\Omega}_1 \cup \overline{\Omega}_2 = \overline{\Omega}$ and $\Omega_1 \cap \Omega_2 = \emptyset$. The *interface* between the two domains, $\sigma = \overline{\Omega}_1 \cap \overline{\Omega}_2$, is a connected, non empty set. We want to solve numerically the elliptic boundary value problem

$$-\nabla \cdot \mathbf{A}\nabla\varphi + \alpha\varphi = f \text{ in } \Omega, \quad \text{and} \quad \varphi = h \text{ on } \Gamma, \tag{1}$$

using independently defined finite element partitions of Ω_1 and Ω_2, with boundary conditions imposed on each $\Gamma_i = \Gamma \cap \overline{\Omega}_i$ as shown in Figure 1. This computational setting arises in several different contexts. Equations with discontinuous coefficients are ideally formulated as transmission or interface problems with σ aligned to the discontinuity. Another example is solid mechanics in which two deforming bodies come into contact at σ. A third example arises when for practical and efficiency

2000 *Mathematics Subject Classification.* 65F10 (Primary), 65F30 (Secondary).

Sandia is a multiprogram laboratory operated by Sandia Corporation, a Lockheed Martin Company, for the US Department of Energy's National Nuclear Security Administration under contract DE-AC04-94AL85000.

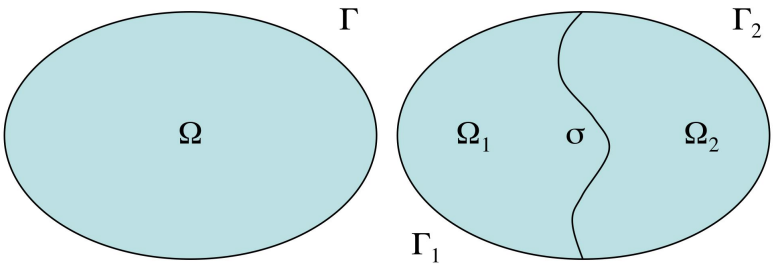

FIGURE 1. The domain Ω is composed of two subdomains, shown on the right.

reasons, grid generation on Ω is replaced by independent meshing of its subdomains. Among other things this approach enables an embarrassingly parallel mesh generation and simplifies meshing of bodies with complex geometries.

1.1. Specifics of mesh tying. In mesh tying Ω is first partitioned into subdomains and then each subdomain is discretized independently. Let Ω_i^h denote a discretization of Ω_i, $i = 1, 2$. The discrete subdomains induce approximations Γ_1^h, Γ_2^h, σ_1^h and σ_2^h of Γ_1, Γ_2 and the interface σ, respectively. Discretization of Ω is given by $\Omega^h = \Omega_1^h \cup \Omega_2^h$. In mesh tying there are two basic configurations for the discrete interfaces σ_1^h and σ_2^h. The first one is when the adjoining surfaces spatially coincide, $\sigma_1^h = \sigma_2^h = \sigma^h$. Typically, this happens when σ is polygonal and can be matched exactly by, e.g., simplexes; see the bottom row in Figure 2. Such interfaces may arise from cutting a complex shape into simpler subdomains to improve efficiency of the mesher. The general case, $\sigma_1^h \neq \sigma_2^h$, typically happens when σ is curved and cannot be represented exactly[1] even by elements with curved sides. This configuration, illustrated in the top row of Figure 2, arises in problems with discontinuous coefficients and contact problems, where the problem definition naturally leads to curved interfaces. In contrast, in domain decomposition and substructuring methods, the discrete domain Ω_h is determined first, and the subdomains are defined *afterwards* as shown in Figure 3. As a result, in these methods the adjoining interfaces always coincide, $\sigma_1^h = \sigma_2^h = \sigma^h$.

A minimal requirement for any mesh-tying or domain bridging method is a consistency condition called *patch test*. A method passes a patch test of order k if it can recover any solution of (1) that is a polynomial of degree k. When $\sigma_1^h \neq \sigma_2^h$ mesh tying methods based on Lagrange multipliers experience difficulties and naively defined schemes fail even a first-order patch test, see [12] for an example. Several approaches have been proposed to address this problem in both two and three dimensions [9, 8, 10, 6, 7, 11, 12]. The methods considered in these papers usually start by selecting one of the non-matching interfaces as a master and the other as a slave surface. The approach of [8, 9, 10] defines Lagrange multipliers on the slave

[1]While finite element methods routinely replace curved boundaries Γ by polygonal approximations Γ^h, the situation is fundamentally different when a curved interface σ is replaced by two spatially distinct discrete interfaces σ_1^h and σ_2^h. While both cases can be viewed as variational crimes in the sense of [14, p.193], the former case leads to a perturbation of the original problem that can be estimated by the Strang's lemma [14, Lemma 4.1, p.186]. For polygonal approximations the error in energy is $O(h^3)$; see [14, p.196]. In the latter case, the discrete computational domain $\Omega_1^h \cup \Omega_2^h$ has gaps and overlaps where the problem ceases to be well-defined. In the overlap regions the 'solution' is multiple valued, and in the voids it is undefined.

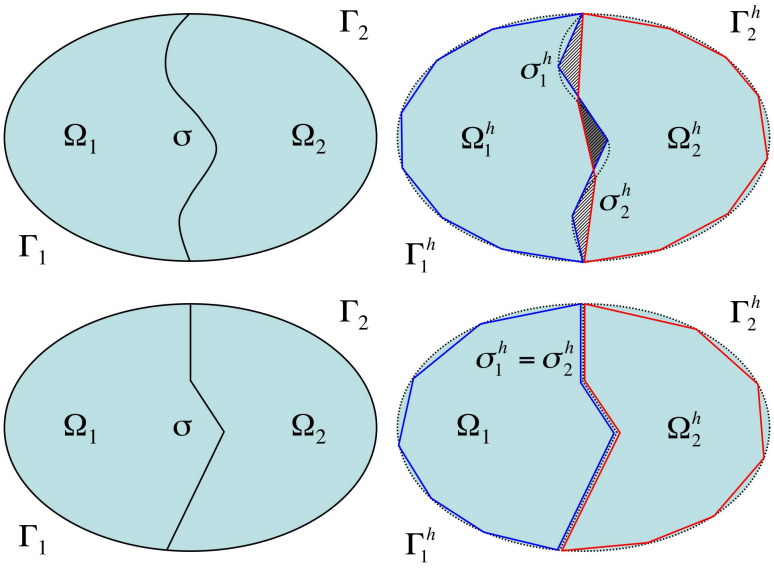

FIGURE 2. In mesh tying subdomains are defined before discretizations. When σ is curved the discrete subdomains may have spatially non-coincident interfaces (top row). When σ is polygonal, interfaces will match (bottom row). The overlap region is shown in black and the void region is shown in gray.

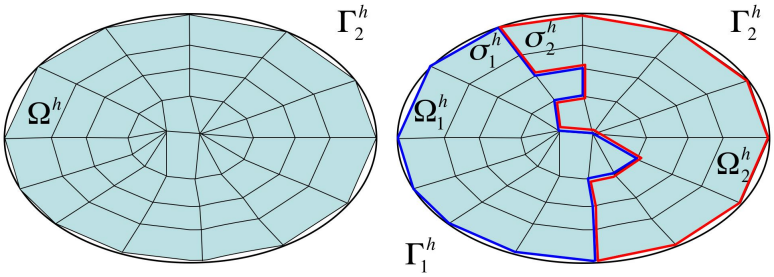

FIGURE 3. In domain decomposition subdomains are defined after partition of Ω and their adjoining surfaces are spatially coincident

surface and uses a projection operator from the master surface. The mesh tying approaches considered in [6, 7, 11, 12] build additional mesh structures between the slave and master interfaces using tools that range from mesh imprinting to local L^2 projections.

In contrast, our approach for dealing with non-matching interfaces utilizes least-squares principles and extends a least-squares method for transmission problems (see Section 2 or [5]), where $\sigma_1^h = \sigma_2^h$, to problems where $\sigma_1^h \neq \sigma_2^h$. Originally, least-squares methods were conceived as a way to recover the desirable Rayleigh-Ritz setting even in cases when the boundary value problem could not be associated with unconstrained optimization of a quadratic energy functional. A least-squares functional is defined as the sum of the residuals of the differential equations measured in the norm of some Sobolev space. As a result, such a functional always

vanishes at the exact solution. By exploiting this property, a least-squares method for mesh tying is formulated that automatically passes a patch test of the same order as the finite element space employed in its definition. We start by perturbing the discrete interfaces until there are no void regions between the subdomains. Then, least-squares principles for each subdomain are joined together by generalized jump terms defined on the overlap region between the subdomains. By measuring residual energy and not physical energy, a least-squares functional may measure energy redundantly in subdomain intersections. This redundancy greatly simplifies the algorithm. Methods that minimize physical energy subject to appropriate constraints on the interfaces, on the other hand, require additional meshing and bookkeeping to avoid counting energy twice in the overlap regions.

The contents of the paper are as follows. In the next section we introduce the notation used throughout the paper. For the convenience of the reader, the method of [5] is summarized in Section 2. The extension to non-matching interfaces is presented in Section 3. Numerical examples illustrating the consistency of the least squares mesh tying method are discussed in Section 4.

1.2. Notations. Our focus is on mesh tying for the case of non-matching interfaces. For clarity, throughout the paper we assume that Ω is such that $\Gamma^h = \Gamma$ and Ω_i^h match their continuous counterparts everywhere except along the interface σ:

$$\Gamma_i^h = \Gamma_i \quad \text{but} \quad \sigma_1^h \neq \sigma_2^h \,,$$

where $\sigma_i^h = \partial\Omega_i^h / \Gamma_i^h$. The *void* and *overlap* regions between Ω_1^h and Ω_2^h are

$$\Omega_V = \Omega / (\overline{\Omega}_1^h \cup \overline{\Omega}_2^h) \quad \text{and} \quad \Omega_O = \Omega_1^h \cap \Omega_2^h \,,$$

respectively. We assume that

$$\overline{\Omega} = (\overline{\Omega}_1^h / \Omega_O) \cup (\overline{\Omega}_2^h / \Omega_O) \cup \overline{\Omega}_O \cup \overline{\Omega}_V \,. \tag{2}$$

Variational settings will be discussed in terms of standard finite element notation. As usual, $L^2(\mathcal{D})$ will stand for the Hilbert space of all square integrable functions defined over a domain $\mathcal{D}$. Similarly $H(\mathrm{div}, \mathcal{D})$ will stand for the Hilbert space of all functions in $(L^2(\mathcal{D}))^n$ with square integrable divergence, equipped with the norm

$$\|\mathbf{v}\|_{\mathrm{div},\mathcal{D}} = \left(\|\mathbf{v}\|_{0,\mathcal{D}}^2 + \|\nabla \cdot \mathbf{v}\|_{0,\mathcal{D}}^2 \right)^{1/2} .$$

For $k > 0$, $H^k(\mathcal{D})$ denotes the subspace of $L^2(\mathcal{D})$ that consists of all functions having square integrable derivatives up to order k. The space $H_0^1(\mathcal{D})$ contains all functions in $H^1(\mathcal{D})$ that vanish on $\partial\mathcal{D}$. In situations when $\partial\mathcal{D}$ is partitioned into two disjoint pieces Γ and σ, we will use $H_\Gamma^1(\mathcal{D})$ to denote all functions in $H^1(\mathcal{D})$ that vanish on Γ only. The inner product and norm on $H^k(\mathcal{D})$ are denoted by $(\cdot,\cdot)_{k,\mathcal{D}}$ and $\|\cdot\|_{k,\mathcal{D}}$, respectively.

To discuss least squares for mesh tying we need the tensor product space

$$\mathbf{H}^1 = \{\varphi = (\varphi_1, \varphi_2) \,|\, \varphi_i \in H^1(\Omega_i);\ i = 1, 2\} \,, \tag{3}$$

its subspace $\mathbf{H}_0^1$ consisting of pairs $(\varphi_1, \varphi_2) \in H_{\Gamma_1}^1(\Omega_1) \times H_{\Gamma_2}^1(\Omega_2)$ that vanish on Γ_i, and the space

$$\mathbf{H}(\mathrm{div}) = \{\mathbf{v} = (\mathbf{v}_1, \mathbf{v}_2) | \mathbf{v}_i \in H(\Omega_i, \mathrm{div});\ i = 1, 2)\}. \tag{4}$$

The spaces $\mathbf{H}^1$ and $\mathbf{H}(\mathrm{div})$ equipped with the inner products

$$\ll \varphi, \psi \gg_1 = \sum_{i=1}^{2} (\varphi_i, \psi_i)_{1,\Omega_i} \quad \text{and} \quad \ll \mathbf{u}, \mathbf{v} \gg_{\mathrm{div}} = \sum_{i=1}^{2} (\mathbf{u}_i, \mathbf{v}_i)_{\mathrm{div},\Omega_i} \,,$$

respectively, are Hilbert spaces. Their norms are denoted by $|||\cdot|||_1$ and $|||\cdot|||_{\rm div}$.

2. A least-squares methods for transmission problems

Consider a symmetric and positive definite matrix function $\mathbf{A}$ that is continuous in Ω with the exception of a piecewise smooth surface σ that divides Ω into two simply connected sub-domains Ω_1 and Ω_2, see Figure 1. We consider least-squares methods for the transmission problem

$$-\nabla\cdot\mathbf{A}_k\nabla\varphi_i+\alpha_i\varphi_i = f_i \quad \text{in } \Omega_i,\ i=1,2, \tag{5}$$

$$\varphi_i = 0 \quad \text{on } \Gamma_i,\ i=1,2, \tag{6}$$

$$\varphi_1 = \varphi_2 \quad \text{on } \sigma. \tag{7}$$

where $\mathbf{A}_i=\mathbf{A}|_{\Omega_i}$ and f_i are given source terms. Standard least-squares methods [3] formulate (5) as the equivalent first-order system

$$\nabla\cdot\mathbf{u}_i+\alpha_i\varphi_i=f_i \quad\text{and}\quad \mathbf{u}_i+\mathbf{A}_i\nabla\varphi_i=0 \quad \text{in } \Omega_i,\ i=1,2 \tag{8}$$

augmented with the boundary condition (6), the interface condition (7) and the additional flux balance condition

$$\mathbf{u}_1\cdot\mathbf{n}_1+\mathbf{u}_2\cdot\mathbf{n}_2=0\,. \tag{9}$$

The least-squares method for the transmission problem is formulated in the case that Ω_1^h and Ω_2^h have a matching interface, $\sigma^h=\sigma_1^h=\sigma_2^h$ (see Section 3 for the non-matching case). Let

$$[\psi]=\psi_1-\psi_2 \quad\text{and}\quad [\mathbf{v}]=\mathbf{v}_1\cdot\mathbf{n}_1+\mathbf{v}_2\cdot\mathbf{n}_2$$

and $\mathbf{H}^h$ denote a finite element subspace of $\mathbf{H}=\mathbf{H}_0^1\times\mathbf{H}(\mathrm{div})$. Gunzburger and Cao [5] proposed to solve (5)-(7) numerically by minimizing the quadratic functional

$$\begin{aligned} J_h(\psi^h,\mathbf{v}^h;f) = \frac{1}{2}\sum_{i=1}^{2}\left(\|\nabla\cdot\mathbf{v}_i^h+\alpha_i\psi_i-f_i\|^2_{0,\Omega_i^h}+\|\mathbf{v}_i^h+\mathbf{A}_i\nabla\psi_i^h\|^2_{0,\Omega_i^h}\right)\\ +\frac{1}{2h^{1+\varepsilon_0}}\int_{\sigma^h}[\psi^h]^2ds+\frac{1}{2h^{\varepsilon_1}}\int_{\sigma^h}[\mathbf{v}^h]^2ds \end{aligned} \tag{10}$$

over $\mathbf{H}^h$. Note that the functional J_h is mesh-dependent and is only defined over finite dimensional subspaces $\mathbf{H}^h$ of $\mathbf{H}_0^1\times\mathbf{H}(\mathrm{div})$ parameterized by h. The values of ε_0 and ε_1 are real parameters that can be adjusted to improve convergence.

A similar method, but based on least-squares principle for the second order problem (5) was considered by Aziz *et al* [1]. This method requires conforming subspaces of $\mathbf{H}^2$ that are more difficult to construct on general unstructured grids.

The minimizer of (10) is the solution $(\varphi^h,\mathbf{u}^h)\in\mathbf{H}^h$ of the Euler equation:

$$B^h(\varphi^h,\mathbf{u}^h;\psi^h,\mathbf{v}^h)=F^h(\psi^h,\mathbf{v}^h)\quad\forall(\psi^h,\mathbf{v}^h)\in\mathbf{H}^h. \tag{11}$$

The bilinear form for $J_h(\psi^h,\mathbf{v}^h;f)$ is

$$\begin{aligned} B^h(\varphi^h,\mathbf{u}^h;\psi^h,\mathbf{v}^h) = \sum_{i=1}^{2}\left(\nabla\cdot\mathbf{u}_i^h+\alpha_i\varphi_i,\nabla\cdot\mathbf{v}_i^h+\alpha_i\psi_i\right)_{0,\Omega_i^h}\\ +\sum_{i=1}^{2}\left(\mathbf{u}_i^h+\mathbf{A}_i\nabla\varphi_i^h,\mathbf{v}_i+\mathbf{A}_i\nabla\psi_i\right)_{0,\Omega_i^h}\\ +\frac{1}{h^{1+\varepsilon_0}}\int_{\sigma^h}[\varphi^h][\psi^h]\,ds+\frac{1}{h^{\varepsilon_1}}\int_{\sigma^h}[\mathbf{u}^h][\mathbf{v}^h]\,ds \end{aligned} \tag{12}$$

and the right hand side functional is $F^h(\psi^h,\mathbf{v}^h)=\sum_i(f_i,\nabla\cdot\mathbf{v}_i^h)_{0,\Omega_i^h}+(f_i,\psi_i^h)_{0,\Omega_i^h}$.

The least-squares method (11) is well understood. Under some reasonable assumptions Gunzburger and Cao [5] proved that for any proper subspace $\mathbf{H}^h$ of $\mathbf{H}$ the bilinear form (12) is coercive on $\mathbf{H}^h \times \mathbf{H}^h$. In particular, coercivity holds if the scalar and the vector variables on each sub-domain are approximated by the same finite element spaces. For example, we can use piecewise linear elements to approximate all unknown fields. Other discretization choices are also possible. Bochev and Gunzburger [4] have shown that by using $H(\mathrm{div})$ conforming elements for the flux the least-squares method acquires some additional properties such as local conservation. We will not consider this type of elements for $\mathbf{H}^h$ in this paper. Coercivity of the bilinear form $B(\cdot,\cdot)$ implies that the weak equation (11) has a unique solution. The jump terms in (10) are computed using field expansions from each sub-domain, and so the grids on σ_1^h and σ_2^h are not required to match. Note that in mortar methods a separate grid on σ^h may be required for the discrete Lagrange multiplier.

3. Least squares method for mesh tying

A least-squares method for spatially non-coincident interfaces is developed next. In order to focus the discussion on a simple type of mesh tying instead of general transmission problems, we assume that $\mathbf{A}$ is the identity and $\alpha \equiv 1$. When $\sigma_1^h \neq \sigma_2^h$ the main problem with (10) is the definition of the interface jump terms. To motivate our approach, note that these terms can be viewed as a "glue" that is applied to the common interface to hold together the sub-domain problems. When the surfaces don't match but there's a sufficient overlap Ω_O between the sub-domains, they can be joined together by applying the glue to the overlap region. Variational realization of this "glue" are the generalized jump terms

$$\|\varphi_1^h - \varphi_2^h\|^2_{1,\Omega_O} \quad \text{and} \quad \|\mathbf{v}_1^h - \mathbf{v}_2^h\|^2_{\mathrm{div},\Omega_O}\,, \tag{13}$$

respectively, which replace the standard interface jump terms in (10). Because a least-squares functional measures residual rather than physical energy, there's no need to subtract energy from Ω_O.

3.1. The mesh tying region. Our least-squares functional is defined in the case of overlapping regions, $\Omega_V = \emptyset$. If the intersection $\sigma^h = \sigma_1^h \cap \sigma_2^h$ is nontrivial, then the corresponding terms in the least-squares for transmission problems apply in σ^h. In the case of non-coincident sub-domains we propose to augment the least-squares functional (10) by adding the generalized jump terms (13). We define the mesh tying 'region' as

$$\Sigma^h = \Omega_O \cup \sigma^h = \overline{\Omega}_1^h \cap \overline{\Omega}_2^h. \tag{14}$$

In words Σ^h is the union of the overlap region and any spatially coincident segments of the discrete interfaces.

If Ω_i^h are such that $\Omega_V \neq \emptyset$ we proceed as follows to perturb the interface to close the voids. Bear in mind that in the case of polygonal domains and quasi-uniform meshes, the diameter of the overlap and void regions is $O(h^2)$. Let $N(\sigma_i^h)$ denote the set of all vertices on interface σ_i^h, $i = 1, 2$ that are not on the Dirichlet boundary Γ. For each vertex $\mathbf{z}_i \in N(\sigma_i^h)$ we consider a perturbation $\delta\mathbf{z}_i$ and define the perturbed subdomains $\widehat{\Omega}_i^h$ by changing $\mathbf{z}_i \in N(\sigma_i^h)$ to $\mathbf{z}_i + \delta\mathbf{z}_i$. Note that the only elements in $\widehat{\Omega}_i^h$ that differ from the elements in Ω_i^h are those that have a vertex on the interface. We assume that Ω_i^h are such that there exist perturbations $\delta\mathbf{z}$ with the following properties; see Figure 4:

(1) The void region, Ω_V, of the perturbed subdomains is empty.

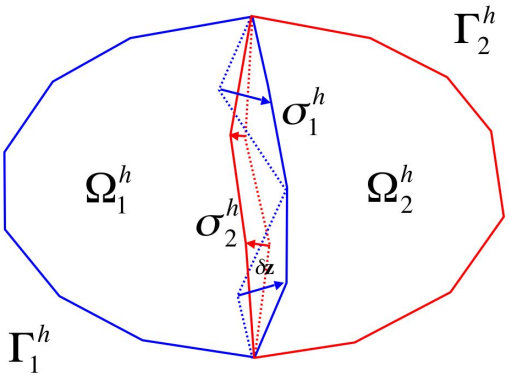

FIGURE 4. Interface perturbations give sub-domains with no gaps between them.

(2) The overlap region $\widehat{\Omega}_O = \widehat{\Omega}_1^h \cap \widehat{\Omega}_2^h \neq \emptyset$ or if $\widehat{\Omega}_O = \emptyset$, then $\sigma_1^h = \sigma_2^h = \sigma^h$.
(3) All perturbed elements in $\widehat{\Omega}_i^h$ are non-degenerate.

The hypothesis that $\Omega_V = \emptyset$ is satisfied by defining Σ^h as in (14), but in terms of the perturbed subdomains. In most situations of practical interest, the above conditions can be easily met. An example of domain perturbation used in our numerical experiments is given in Section 4. In some cases, such as an interface σ containing a polygonal subregion, perturbations such that $\sigma_1^h \cap \sigma_2^h$ is nontrivial are available. The overlap region Ω_O may not be simply connected. However, it is important to note that the purpose of the interface node perturbations is not to match the interfaces (which in general is impossible), but only to eliminate the void region. Mesh imprinting techniques are much more complicated.

3.2. A least-squares principle for mesh tying. In what follows $\mathbf{H}^1$ and $\mathbf{H}(\mathrm{div})$ denote the spaces (3) and (4) defined with respect to Ω_1^h and Ω_2^h. The least-squares functional J_h on the finite element subspace $\mathbf{H}^h$ of $\mathbf{H}^1 \times \mathbf{H}(\mathrm{div})$ considered here is

$$
\begin{aligned}
J_h(\psi^h, \mathbf{v}^h; f) = \frac{1}{2}\Big(&\sum_{i=1}^{2} \|\nabla\cdot \mathbf{v}_i^h + \psi_i^h - f_i\|^2_{0,\Omega_i^h} + \|\mathbf{v}_i^h + \nabla\psi_i^h\|^2_{0,\Omega_i^h} \\
&+ \frac{1}{h^{1+\varepsilon_0}}\int_{\sigma^h} [\psi^h]^2\, ds + \frac{1}{h^{\varepsilon_1}}\int_{\sigma^h} [\mathbf{v}^h]^2\, ds\Big) \\
&+ \omega_\phi \|\psi_1^h - \psi_2^h\|^2_{1,\Omega_O} + \omega_{\mathbf{v}} \|\mathbf{v}_1^h - \mathbf{v}_2^h\|^2_{\mathrm{div},\Omega_O}\,,
\end{aligned}
\tag{15}
$$

where σ^h is the set from (14). The first two lines in (15) coincide with the least squares functional (10) for the transmission problem. The last line contains terms that can be viewed as the proper extensions of the jump terms to the overlap regions. The weights ω_ϕ and $\omega_{\mathbf{v}}$ are positive real numbers that are independent of the mesh size h. The least-squares principle for (15) is

$$
\min_{(\psi^h,\mathbf{v}^h)\in\mathbf{H}^h} J_h(\psi^h, \mathbf{v}^h; f).
\tag{16}
$$

The finite element minimizer $(\varphi^h, \mathbf{u}^h) \in \mathbf{H}^h$ of (16) solves the Euler equation

$$
B_\Sigma^h(\varphi^h, \mathbf{u}^h; \psi^h, \mathbf{v}^h) = F_\Sigma^h(\psi^h, \mathbf{v}^h) \quad \forall (\psi^h, \mathbf{v}^h) \in \mathbf{H}^h.
\tag{17}
$$

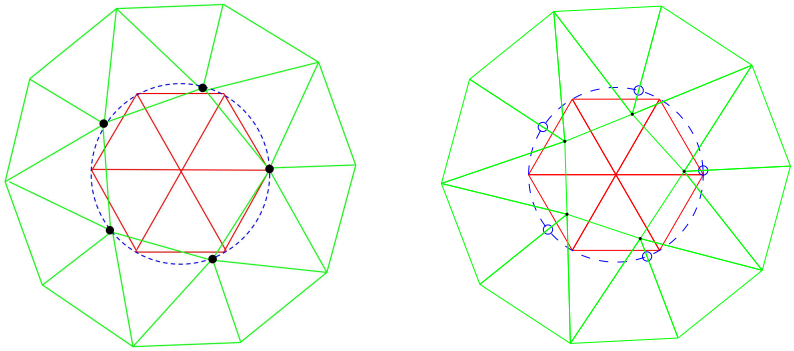

FIGURE 5. Computational domains Ω_1^h (red) and Ω_2^h (green) used in the numerical experiments. The dotted line is the true curved interface σ. The left plot shows the discretized sub-domains before the perturbation. The void regions are clearly visible. The right plot shows the sub-domains after the perturbation to remove the gaps. The nodes on the interior disk Ω_1^h are not perturbed. The interface nodes on the annulus Ω_2^h are perturbed. The circles mark the original interface node locations.

The bilinear form and functional in (16) are given by

$$
\begin{aligned}
&B_\Sigma^h(\varphi^h, \mathbf{u}^h; \psi^h, \mathbf{v}^h) \\
&\quad = \sum_{i=1}^{2} \left(\nabla\cdot\mathbf{u}_i^h + \varphi_i, \nabla\cdot\mathbf{v}_i^h + \psi_i\right)_{0,\Omega_i^h} + \left(\mathbf{u}_i^h + \nabla\varphi_i^h, \mathbf{v}_i + \nabla\psi_i\right)_{0,\Omega_i^h} \\
&\quad + \frac{1}{h^{1+\varepsilon_0}} \int_{\sigma^h} [\varphi^h][\psi^h]\, ds + \frac{1}{h^{\varepsilon_1}} \int_{\sigma^h} [\mathbf{u}^h][\mathbf{v}^h]\, ds \\
&\quad + \omega_\phi \left(\varphi_1^h - \varphi_2^h, \psi_1^h - \psi_2^h\right)_{1,\Omega_O} + \omega_{\mathbf{v}} \left(\mathbf{u}_1^h - \mathbf{u}_2^h, \mathbf{v}_1^h - \mathbf{v}_2^h\right)_{\mathrm{div},\Omega_O}
\end{aligned}
\tag{18}
$$

and $F_\Sigma^h(\psi^h, \mathbf{v}^h) = \sum_i (f_i, \nabla\cdot\mathbf{v}_i^h)_{0,\Omega_i^h} + (f_i, \psi_i^h)_{0,\Omega_i^h}$, respectively.

The analysis of the mesh tying least-squares method, including the automatic passage of patch tests of all orders, will be presented in the forthcoming paper [2]. Motivated by the analysis in this paper we choose $\omega_\phi = \omega_{\mathbf{v}} = 3$.

4. Implementation and numerical results

In this section we briefly comment on the computational geometry used in the sub-domain perturbations that eliminate the void. Then we present some numerical experiments with the least-squares mesh tying method. In all experiments the computational domain Ω is a disk of radius two. It is partitioned into a disk of radius one (the sub-domain Ω_1) and an annulus (the sub-domain Ω_2); see Fig. 5. Linear systems were solved using MATLAB's sparse direct Cholesky factorization algorithm.

4.1. Sub-domain perturbations and assembly. To discretize Ω_1 and Ω_2 we used the grid generation package Triangle [13]. The initial discrete subdomains Ω_1^h and Ω_2^h represented polygonal approximations of the disk and the annulus. Because our goal was to test the mesh tying least-squares method for overlapping domains,

the mesh was generated in such a way that σ_1^h and σ_2^h were two distinct interfaces; see Fig. 5.

The complexity of the finite precision arithmetic computational geometry required to determine the overlap domain was reduced by using two simplifications. First, in all the meshes used no interface edge was refined from the input curves. Second, in the numerical experiments the overlap regions were always contained in the union of the elements from either domain with an interface vertex. Furthermore, for our geometry, only the interface nodes on the annulus are perturbed. The nodes are perturbed until they intersect the opposite boundary, and then a small amount more.

To assemble the matrix for the least-squares problem in (16) some interpolation was required in the overlap regions to compute the element contributions from the generalized jump terms (13). The triangle intersection triangulations needed for this purpose were determined using a shortest edge criterion.

4.2. Patch test and convergence studies. We show results for a patch test using piecewise linear elements. We carried out experiments on different combinations of grids for Ω_1^h and Ω_2^h that had different amounts of overlap (after perturbations). A representative example of our patch test is shown in Fig. 6. The exact solution is $\varphi(x, y) = y$. The Dirichlet data on the discrete boundary $\partial\Omega^h$ is set by evaluating the exact solution at the boundary nodes. The plots show that the least-squares mesh tying method recovers the exact solution and its derivatives. The width of the overlap had no impact on the outcomes of the patch tests.

We conclude this section with a convergence study of the least-squares mesh tying method. The convergence results shown below were obtained by using a manufactured solution given by the first eigenfunction of the partial differential equation for Dirichlet boundary conditions. The eigenfunctions are radially symmetric and have representations in terms of Bessel's function of the first kind of order zero, $j_0(r)$. Specifically, $-\Delta\varphi + \varphi = \varphi(1 + \omega^2)$, for $\varphi(x, y) = j_0(r\omega/2)$, $r = \sqrt{x^2 + y^2}$ and $\omega = 2.404825557695707\ldots$. In the mesh convergence studies, the finest meshes were determined by uniform mesh refinement from coarser meshes.

One can show that on a sub-domain Ω_i^h the least-squares functional (15) is equivalent to the energy norm $\|\mathbf{v}\|_{div,\Omega_i^h} + \|\varphi\|_{1,\Omega_i^h}$. (For the norm equivalence properties of the functional on $\Omega_h^1 \cap \Omega_2^h$ we refer to [2].) Therefore, for piecewise linear elements we expect to observe linear convergence rates for the H^1 and $H(\mathrm{div})$ semi-norm errors in the scalar and the vector variables, respectively. Our results are shown in Fig. 7. In this figure, errors are reported separately for each one of the sub-domains. We see that as the mesh is refined, errors on both sub-domains become closely clustered and converge at approximately the same linear rate. While the amount of overlap did not prove important for passing the linear patch test, we found that it had some effect on the numerical convergence rates. Results on Fig. 7 were obtained with overlap of width $h/6$. Preliminary experiments with minimal $h^{1.75}/6$ overlap produced slightly lower convergence rates.

5. Conclusions

A least-squares mesh tying method is presented in Section 3 for the partial differential equation $-\nabla^2\varphi + \alpha\varphi = f$ posed over a domain that consists of two overlapping subdomains. The corresponding finite element meshes are non-coincident. The least-squares functional ties the meshes together across the curved interface covered by the subdomains intersection. Advantages of the formulation, including patch test consistency and optimal convergence rates, are demonstrated.

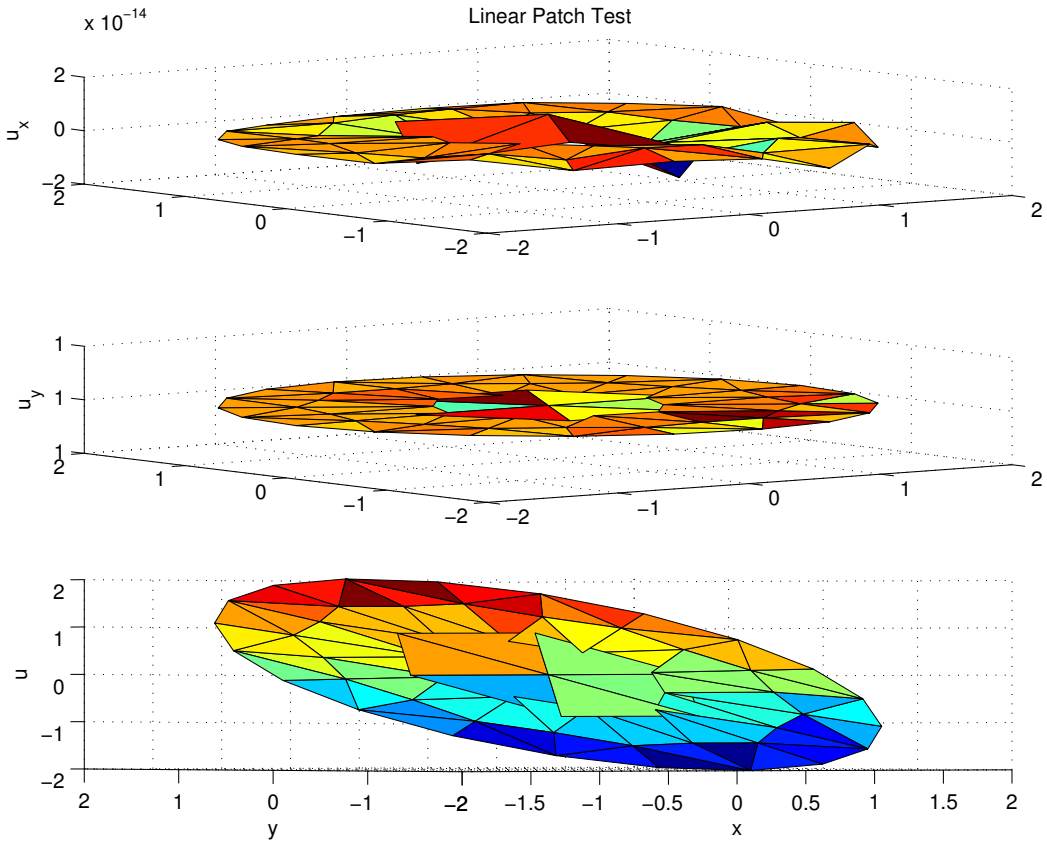

FIGURE 6. Results for the patch test with solution $u(x, y) = y$ are displayed. The top two figures show the components of the gradient, and bottom figure shows the displacement. The solution is exact to within round off error. In the top figure the vertical scale is from -5×10^{-15} to 5×10^{-15}. The overlap region is visible in the bottom figure.

Acknowledgment

This paper is dedicated to the occasion of Max Gunzburger's 60th birthday. The first author wishes to express his deepest gratitude to Max, who patiently taught him about finite elements, least-squares and the finer points of being a computational mathematician. The authors also wish to thank their colleagues C. Dohrmann and M. Heinstein for sharing their experience about mesh tying.

References

[1] A. Aziz, R. Kellogg, and A. Stephens. Least-squares methods for elliptic systems. *Math. Comp.*, 44(169):53–70, 1985.

[2] P. Bochev and D. Day. Analysis of a least-squares mesh tying method. In preparation, 2006.

[3] P. Bochev and M. Gunzburger. Finite element methods of least-squares type. *SIAM Review*, 40/4:789–837, 1998.

[4] P. Bochev and M. Gunzburger. On least-squares finite element methods for the Poisson equation and their connection to the Dirichlet and Kelvin principles. *SIAM J. Numer. Anal.*, 43:340–362, 2005.

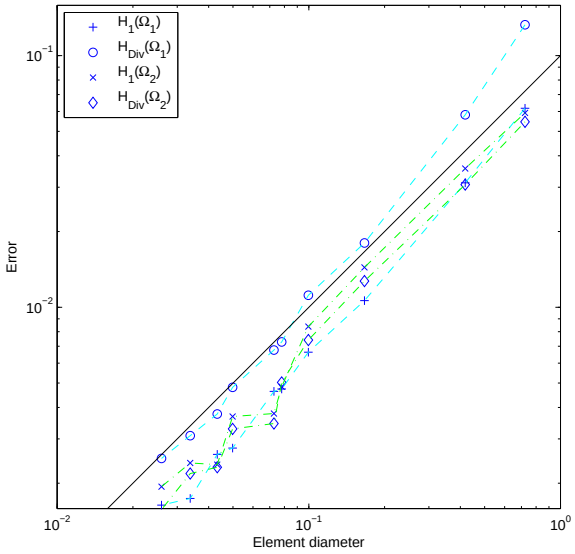

FIGURE 7. Plots of $|\mathbf{u}_i^h - \mathbf{u}_i|_{\text{div}}$ and $|\varphi_i^h - \varphi|_1$ for subdomains $i = 1, 2$. The o and $+$ curves correspond to the $H(\text{div})$ and H^1 semi-norms on the inner disk Ω_1^h respectively. The $\diamondsuit$ and $\times$ curves correspond to the $H(\text{div})$ and H^1 semi-norms on the annular domain Ω_2^h respectively. The solid line has equation $e(h) = h/10$ and is included for reference.

[5] Y. Cao and M. Gunzburger. Least-squares finite element approximations to solutions of interface problems. *SIAM J. Numer. Anal.*, 35(1):393–405, 1998.
[6] C. R. Dohrmann, S. W. Key, and M. W. Heinstein. A method for connecting dissimilar finite element meshes in two dimensions. *Int. J. Numer. Meth. Engng.*, 48:655–678, 2000.
[7] C. R. Dohrmann, S. W. Key, and M. W. Heinstein. Methods for connecting dissimilar three-dimensional finite element meshes. *Int. J. Numer. Meth. Engng.*, 47:1057–1080, 2000.
[8] B. Flemisch, J.M. Melenk, and B.I. Wohlmuth. Mortar methods with curved interfaces. *Appl. Numer. Math.*, 54(3-4):339–361, 2005.
[9] B. Flemisch, M.A. Puso, and B.I. Wohlmuth. A new dual mortar method for curved interfaces: 2D elasticity. *Internat. J. Numer. Methods Engrg.*, 63(6):813–832, 2005.
[10] B. Flemisch and B.I. Wohlmuth. Stable Lagrange multipliers for quadrilateral meshes of curved interfaces in 3D, IANS preprint 2005/005. Technical report, University of Stuttgart, 2005.
[11] M. W. Heinstein and T. A. Laursen. A three dimensional surface-to-surface projection algorithm for non-coincident domains. *Commun. Numer. Meth. Engng.*, 19:421–432, 2003.
[12] T. A. Laursen and M. W. Heinstein. Consistent mesh tying methods for topologically distinct discretized surfaces in non-linear solid mechanics. *Int. J. Numer. Meth. Engng.*, 57:1197–1242, 2003.
[13] J. R. Shewchuk. Delaunay refinement algorithms for triangular mesh generation. *Comp. Geom. Theory and Apps.*, 22:21–74, 2002.
[14] G. Strang and G. Fix. *An analysis of the finite element method*. Prentice Hall, New Jersy, 1973.

Computational Mathematics and Algorithms Department, Sandia National Laboratories, P.O. Box 5800, Albuquerque, NM 87185-1110
E-mail: pbboche@sandia.gov

Computational Mathematics and Algorithms Department, Sandia National Laboratories, P.O. Box 5800, Albuquerque, NM 87185-1110
E-mail: dmday@sandia.gov